Journal of Solid State Chemistry **164,** 367–373 (2002)
doi:10.1006/jssc.2001.9510, available online at http://www/idealibrary.com on IDEAL®

Structures and Magnetic Properties of Iron Diphosphonates: $[NH_3(CH_2)_2NH_3][Fe^{II}\{HO_3PC(CH_3)(OH)(PO_3H)\}_2]\cdot 2H_2O$ and $[NH_3(CH_2)_2NH_2(CH_2)_2NH_3][Fe^{III}\{O_3PC(CH_3)(OH)(PO_3H)\}_2]\cdot H_2O$

Hui-Hua Song,* Li-Min Zheng,*[,1] Guangshan Zhu,† Zhan Shi,† Shouhua Feng,† Song Gao,‡ Zheng Hu,* and Xin-Quan Xin*

*State Key Laboratory of Coordination Chemistry, Department of Chemistry, Nanjing University, Nanjing 210093, Peoples Republic of China; †State Key Laboratory of Inorganic Synthesis and Preparative Chemistry, Department of Chemistry, Jilin University, Changchun 130023, People's Republic of China; and ‡State Key Lab of Rare Earth Materials Chemistry and Applications, Peking University, Beijing 100870, People's Republic of China

Received October 4, 2001; in revised form December 21, 2001; accepted January 11, 2002

Two iron diphosphonates, $[NH_3(CH_2)_2NH_3][Fe^{II}\{HO_3PC(CH_3)(OH)(PO_3H)\}_2]\cdot 2H_2O$ (1) and $[NH_3(CH_2)_2NH_2(CH_2)_2NH_3][Fe^{III}\{O_3PC(CH_3)(OH)(PO_3H)\}_2]\cdot H_2O$ (2), have been synthesized under hydrothermal conditions. Crystal data: 1, monoclinic, $C2/c$, $a=24.754(5)$, $b=5.331(1)$, $c=16.010(3)$ Å, $\beta=117.787(3)^\circ$, $V=1868.9(6)$ Å^3, $Z=4$, $R1=0.0321$; 2, orthorhombic, $Pbcn$, $a=22.128(4)$, $b=9.9479(9)$, $c=19.110(2)$ Å, $V=4206.7(9)$ Å^3, $Z=8$, $R1=0.0389$. Both show chain structures in which anionic chains of $[Fe^{II}\{HO_3PC(CH_3)(OH)(PO_3H)\}_2]_n^{2n-}$ in 1 or $[Fe^{III}\{O_3PC(CH_3)(OH)(PO_3H)\}_2]_n^{3n-}$ in 2 are composed of $\{Fe^{II}O_6\}$ or $\{Fe^{III}O_6\}$ octahedra and $\{CPO_3\}$ tetrahedra alternatively. The protonated organic amines and lattice water are located between the chains with extensive hydrogen bonding interactions. Weak antiferromagnetic exchange couplings are propagated between the magnetic centers through the O–P–O bridges in both cases. © 2002 Elsevier Science (USA)

Key Words: **iron diphosphonate; 1-hydroxyethylidenediphosphonate; magnetic properties.**

INTRODUCTION

In recent years, the exploration of new transition metal phosphonate compounds has gained an increased attention due to their potential applications in ion exchanges, absorptions and sensors (1–6). Among the great efforts made in this area, compounds containing iron(II) or iron(III) are still rather limited in number, including $HFe^{III}(C_6H_5PO_3H)_4$, $HFe^{III}(RPO_3)_2\cdot H_2O$ ($R=C_2H_5$, C_6H_5), $HFe^{III}(CH_3PO_3)_2$ (7–9), $Fe^{II}(C_2H_5PO_3)\cdot H_2O$ (10), $[Fe_2^{III}(H_2O)_2(O_3PCH_2PO_3H)_2](H_2O)_2$ (11), and $Fe_2^{II}(O_3PCH_2CH_2PO_3)\cdot 2H_2O$ (12). Their structures are either one-dimensional, as in $HFe^{III}(C_6H_5PO_3H)_4$, or two- or three-dimensional, as found in the latter three compounds.

By using 1,4-butylenediamine as a structure-directing agent, we have succeeded in synthesizing an Fe(II) diphosphonate, $[NH_3(CH_2)_4NH_3][Fe_2^{II}\{O_3PC(CH_3)(OH)(PO_3H)\}_2]\cdot 2H_2O$, with a novel open-network structure (13). Based on the same 1-hydroxyethylidenediphosphonate [hedp, $O_3PC(CH_3)(OH)PO_3$], two new iron compounds with formulas $[NH_3(CH_2)_2NH_3][Fe^{II}\{HO_3PC(CH_3)(OH)(PO_3H)\}_2]\cdot 2H_2O\cdot$(**1**) and $[NH_3(CH_2)_2NH_2(CH_2)_2NH_3][Fe^{III}\{O_3PC(CH_3)(OH)(PO_3H)\}_2]\cdot H_2O\cdot$(**2**) are reported in this paper. Their magnetic properties are also investigated.

EXPERIMENTAL

Materials and Methods

All the starting materials were reagent grade used as purchased. The aqueous solution of 1-hydroxyethylidenediphosphonic acid (50% $hedpH_4$) was purchased from the Nanjing Shuguang chemical reagent factory. Elemental analyses were performed on a PE 240C elemental analyzer. Infrared spectra were recorded on a IFS66V spectrometer with pressed KBr pellets. Thermal analyses were performed in nitrogen with a heating rate of 5°C/min on a TGA-DTA V1.1B TA Inst 2100 instrument. Mössbauer spectra were carried out with an Austin S-600 Mössbauer spectrometer using a ^{57}Co/Pd source. The instrument was calibrated by a standard sample of $Na_2[Fe(CN)_5(NO)]\cdot 2H_2O$ (SNP) at room temperature. The isomer shifts were reported relative to SNP. Variable-temperature magnetic susceptibility data were obtained on polycrystalline samples (47.8 mg for **1**, 51.5 mg for **2**) from 2 to ca. 300 K in a magnetic field of 5 kOe after zero-field cooling using a MagLab System 2000

[1]To whom correspondence should be addressed. Fax: +86-25-3314502. E-mail: lmzheng@netra.nju.edu.cn.

0022-4596/02 $35.00

magnetometer. Diamagnetic corrections were estimated from Pascal's constants (14).

*Synthesis of $[NH_3(CH_2)_2NH_3][Fe\{HO_3PC(CH_3)(OH)(PO_3H)\}_2]\cdot 2H_2O$ (**1**)*

A mixture of $FeSO_4\cdot 7H_2O$ (1 mmol, 0.2787 g), 50% $hedpH_4$ (5 mmol, 2 cm^3), LiF (1 mmol, 0.0261 g), and H_2O (8 cm^3), adjusted by ethylenediamine to pH ≈3, was transferred directly to a Teflon-lined stainless autoclave (25 cm^3) and heated at 140°C for 48 h. The colorless needle-like crystals were discovered as a monophasic material, judged by powder XRD measurements. (Found: C, 13.16; H, 4.60; N, 5.00. Calcd. for $C_6H_{26}FeN_2O_{16}P_4$: C, 12.82; H, 4.66; N, 5.00%). IR (KBr): 3744m, 3568s, 3151s (br), 1636m, 1541m, 1401m, 1342 w, 1148s, 1073s, 1040s, 925s, 905s, 811m, 780w, 711w, 643w, 557m, 530w, 463w, 446w cm^{-1}.

*Synthesis of $[NH_3(CH_2)_2NH_2(CH_2)_2NH_3][Fe\{O_3PC(CH_3)(OH)(PO_3H)\}_2]\cdot H_2O$ (**2**)*

Hydrothermal treatment of a mixture of $FeSO_4\cdot 7H_2O$ (1 mmol, 0.2787 g), 50% $hedpH_4$ (5 mmol, 2 cm^3), LiF (1 mmol, 0.0258 g), and H_2O (8 cm^3), adjusted by diethylenetriamine to pH ≈3, at 140°C for 48 h resulted in the pale-yellow plate-like crystals as a single phase. (Found: C, 16.88; H, 4.90; N, 7.46. Calcd. for $C_8H_{28}FeN_3O_{15}P_4$: C, 16.38; H, 4.78; N, 7.17%). IR (KBr): 3650 w, 3497s, 3260s(br), 2573m, 2535m, 2375m, 1611m, 1558m, 1523 w, 1472w, 1455w, 1436w, 1408w, 1367w, 1317w, 1212m, 1166s, 1105s, 1034s, 976m, 929m, 910m, 871m, 820m, 682w, 656w, 583m, 562m, 519w, 485w, 413wcm^{-1}.

Fluoride was added in order to improve the crystallization of the final products. The same compounds (**1** and **2**) can be obtained without it.

Crystallographic Studies

Single crystals of dimensions 0.14 × 0.06 × 0.04 mm for **1** and 0.2 × 0.1 × 0.03 mm for **2** were used for structural determinations on a Siemens Smart CCD diffractometer using graphite-monochromated Mo$K\alpha$ radiation ($\lambda = 0.71073$Å) at room temperature. Intensity data were collected in 1271 frames for both compounds. The data were integrated using the Siemens SAINT program (15), with the intensities corrected for Lorentz factor, polarization, air absorption, and absorption due to variation in the path length through the detector faceplate. Number of measured, unique, and observed reflections [$I > 2\sigma(I)$] are 1937, 1288, and 926 ($R_{int} = 0.0323$) for **1**, 8601, 2853, and 2206 ($R_{int} = 0.0366$) for **2**. Empirical absorption and extinction corrections were applied for both compounds.

TABLE 1
Crystallographic Data for 1 and 2

Compound	**1**	**2**
Formula	$C_6H_{26}N_2FeO_{16}P_4$	$C_8H_{28}N_3FeO_{15}P_4$
M	562.02	586.06
Crystal system	monoclinic	orthorhombic
Space group	$C2/c$	$Pbcn$
a/Å	24.754(5)	22.128(4)
b/Å	5.331(1)	9.9479(9)
c/Å	16.010(3)	19.110(2)
β/°	117.787(3)	
V/Å^3	1868.9(6)	4206.7(9)
Z	4	8
D_c/g cm^{-3}	1.997	1.851
F (000)	1160	2424
μ(Mo$K\alpha$)/cm^{-1}	12.36	11.00
Goodness of fit on F^2	0.918	1.007
$R1$, $wR2^a$ [$I > 2\sigma(I)$]	0.0321, 0.0685	0.0389, 0.0995
(all data)	0.0541, 0.0748	0.0533, 0.1088
$(\Delta\rho)_{max}$, $(\Delta\rho)_{min}$/e Å^{-3}	0.358, −0.313	1.301, −0.407

$^a R_1 = \sum ||F_o| - |F_c|| / \sum |F_o| \cdot wR_2 = \left[\sum w(F_o^2 - F_c^2)^2 / \sum w(F_o^2)^2\right]^{1/2}$.

The structures were solved by direct methods and refined on F^2 by full-matrix least squares using SHELXTL (16). The nonhydrogen atoms were refined with anisotropic displacement parameters. All hydrogen atoms were located in difference electron density maps and refined with the isotropic displacement parameters 1.2 or 1.4 times the preceding normal atoms. Crystallographic data are summarized in Table 1, atomic coordinates in Tables 2 and 3, selected bond lengths and angles in Tables 4 and 5.

TABLE 2
Atomic Coordinates and Equivalent Isotropic Displacement Parameters (Å^2) for 1

Atom	x	y	z	U (eq)^a
Fe(1)	0	0	0	0.018(1)
P(1)	0.0630(1)	0.4948(2)	0.1482(1)	0.018(1)
P(2)	0.1248(1)	0.2999(2)	0.0325(1)	0.020(1)
O(1)	0.0109(1)	0.3219(5)	0.0898(2)	0.021(1)
O(2)	0.0564(1)	0.7652(5)	0.1194(2)	0.022(1)
O(3)	0.0765(1)	0.4931(6)	0.2539(2)	0.028(1)
O(4)	0.0756(1)	0.1060(5)	−0.0141(2)	0.022(1)
O(5)	0.1859(1)	0.2310(5)	0.0414(2)	0.025(1)
O(6)	0.1065(1)	0.5560(5)	−0.0215(2)	0.026(1)
O(7)	0.1457(1)	0.1249(6)	0.2022(2)	0.028(1)
O(1W)	0.0723(2)	0.0376(7)	0.3167(2)	0.046(1)
N(1)	0.2101(2)	1.0111(8)	0.4051(3)	0.029(1)
C(1)	0.1325(2)	0.3632(8)	0.1509(3)	0.022(1)
C(2)	0.1868(2)	0.5335(10)	0.2061(4)	0.031(1)
C(3)	0.2294(2)	1.2628(9)	0.4483(3)	0.031(1)

$^a U$(eq) is defined as one third of the trace of the orthogonalized U_{ij} tensor.

TABLE 3
Atomic Coordinates and Equivalent Isotropic Displacement Parameters (Å^2) for 2

Atom	x	y	z	U (eq)[a]
Fe(1)	0.7276(1)	0.5096(1)	0.0954(1)	0.016(1)
P(1)	0.6176(1)	0.3005(1)	0.0479(1)	0.018(1)
P(2)	0.6872(1)	0.2327(1)	0.1819(1)	0.016(1)
P(3)	0.8130(1)	0.2861(1)	0.0093(1)	0.016(1)
P(4)	0.8813(1)	0.2220(1)	0.1449(1)	0.017(1)
O(1)	0.6620(1)	0.4174(2)	0.0399(1)	0.020(1)
O(2)	0.5565(1)	0.3307(3)	0.0194(2)	0.025(1)
O(3)	0.6438(1)	0.1741(3)	0.0089(2)	0.027(1)
O(4)	0.7269(1)	0.3563(3)	0.1650(1)	0.019(1)
O(5)	0.7111(1)	0.1038(3)	0.1498(1)	0.021(1)
O(6)	0.6778(1)	0.2190(3)	0.2596(1)	0.023(1)
O(7)	0.5862(1)	0.3816(3)	0.1744(2)	0.025(1)
O(8)	0.7732(1)	0.1632(2)	0.0274(2)	0.021(1)
O(9)	0.7895(1)	0.4169(2)	0.0401(2)	0.022(1)
O(10)	0.8230(1)	0.2945(2)	−0.0686(2)	0.022(1)
O(11)	0.8404(1)	0.0993(3)	0.1520(1)	0.018(1)
O(12)	0.8511(1)	0.3448(3)	0.1826(2)	0.025(1)
O(13)	0.9429(1)	0.2048(3)	0.1753(2)	0.026(1)
O(14)	0.9127(1)	0.1340(3)	0.0208(2)	0.024(1)
O(1W)	0.9404(2)	0.3237(4)	0.3139(2)	0.059(1)
N(1)	0.5176(2)	0.4863(4)	−0.0989(2)	0.025(1)
C(1)	0.6128(2)	0.2635(4)	0.1421(2)	0.019(1)
N(2)	0.6744(2)	0.5737(4)	−0.1520(2)	0.021(1)
C(2)	0.5694(2)	0.1480(5)	0.1583(3)	0.028(1)
N(3)	0.8415(2)	0.5044(4)	−0.1580(2)	0.024(1)
C(3)	0.8869(2)	0.2553(4)	0.0504(2)	0.019(1)
C(4)	0.9314(2)	0.3683(4)	0.0318(3)	0.028(1)
C(5)	0.5635(2)	0.5657(5)	−0.1370(3)	0.030(1)
C(6)	0.6210(2)	0.4847(4)	−0.1469(3)	0.028(1)
C(7)	0.7315(2)	0.4969(5)	−0.1560(3)	0.031(1)
C(8)	0.7858(2)	0.5877(4)	−0.1558(3)	0.025(1)

[a] U(eq) is defined as one third of the trace of the orthogonalized U_{ij} tensor.

RESULTS AND DISCUSSION

Description of Crystal Structures

Compound **1** shows a chain structure. A fragment of the anionic iron phosphonate chain, $[Fe\{HO_3PC(CH_3)(OH)(PO_3H)\}_2]_n^{2n-}$, is shown in Fig. 1. The coordination geometry around iron is approximately octahedral. Each FeO_6 octahedron shares two pairs of oxygen atoms [O(1) and O(4)] with two equivalent $hedpH_2^{2-}$ groups in a trans mode, forming pentameric units. The remaining two biting sites of FeO_6 are provided by the phosphonate oxygen O(2) from two neighboring pentameric units, leading to a one-dimensional chain. Similar pentameric units have been found in some vanado-methylenediphosphonates (17,18). In the latter cases, however, two- or three-dimensional structures were observed. The Fe–O distances in compound **1** are in the range 2.066(3) to 2.173(3)Å, in agreement with those in $Fe^{II}(C_2H_5PO_3)\cdot H_2O$ [2.05(1)–2.35(1)Å] (10). The bond valence sum calculated for Fe is 2.12 (19).

TABLE 4
Selected Bond Lengths [Å] and Angles [°] for 1

Fe(1)–O(4)	2.066(3)	Fe(1)–O(2B)	2.164(3)
Fe(1)–O(1)	2.173(3)	P(1)–O(2)	1.499(3)
P(1)–O(1)	1.503(3)	P(1)–O(3)	1.566(3)
P(2)–O(5)	1.498(3)	P(2)–O(4)	1.503(3)
P(2)–O(6)	1.566(3)		
O(4A)–Fe(1)–O(4)	180.0(2)	O(4A)–Fe(1)–O(2B)	90.60(10)
O(4)–Fe(1)–O(2B)	89.40(10)	O(4)–Fe(1)–O(2C)	90.60(10)
O(2B)–Fe(1)–O(2C)	180.0(3)	O(4A)–Fe(1)–O(1)	89.04(10)
O(4)–Fe(1)–O(1)	90.96(10)	O(2B)–Fe(1)–O(1)	87.60(10)
O(2C)–Fe(1)–O(1)	92.40(10)	O(1)–Fe(1)–O(1A)	180.00(16)
P(1)–O(1)–Fe(1)	134.54(16)	P(1)–O(2)–Fe(1D)	139.52(18)
P(2)–O(4)–Fe(1)	134.31(16)		

Note. Symmetry transformations used to generate equivalent atoms: A: $-x,-y,-z$; B: $-x,-y+1,-z$; C: $x,y-1,z$; D: $x,y+1,z$.

The $hedpH_2^{2-}$ group functions as a tridentate chelating bridging ligand using three of its six phosphonate oxygens, O(1), O(2), and O(4). Two of the remaining three phosphonate oxygens, O(3) and O(6), are protonated and are involved in the intrachain hydrogen bonds (Table 6). The O(5) atom is pendant. The protonated ethylenediamine and water molecules are located between the $[Fe\{hedpH_2\}_2]_n^{2n-}$ chains, and stabilize the lattice by forming extensive hydrogen bonds with the chain (Fig. 2, Table 6). This compound is isostructural to a related nickel compound, $[NH_3(CH_2)_2NH_3][Ni\{HO_3PC(CH_3)(OH)(PO_3H)\}_2]\cdot 2H_2O$ (20).

TABLE 5
Selected Bond Lengths [Å] and Angles [°] for 2

Fe(1)–O(5A)	1.950(3)	Fe(1)–O(9)	1.960(3)
Fe(1)–O(8A)	2.004(3)	Fe(1)–O(1)	2.016(3)
Fe(1)–O(4)	2.023(3)	Fe(1)–O(11A)	2.056(3)
P(1)–O(2)	1.487(3)	P(1)–O(1)	1.532(3)
P(1)–O(3)	1.573(3)	P(2)–O(6)	1.503(3)
P(2)–O(5)	1.518(3)	P(2)–O(4)	1.547(3)
P(3)–O(10)	1.506(3)	P(3)–O(9)	1.520(3)
P(3)–O(8)	1.546(3)	P(4)–O(13)	1.492(3)
P(4)–O(11)	1.525(3)	P(4)–O(12)	1.567(3)
O(5A)–Fe(1)–O(9)	91.51(11)	O(5A)–Fe(1)–O(8A)	89.14(11)
O(9)–Fe(1)–O(8A)	90.95(11)	O(5A)–Fe(1)–O(1)	178.03(11)
O(9)–Fe(1)–O(1)	90.29(11)	O(8A)–Fe(1)–O(1)	90.03(10)
O(5A)–Fe(1)–O(4)	90.91(11)	O(9)–Fe(1)–O(4)	90.21(11)
O(8A)–Fe(1)–O(4)	178.84(11)	O(1)–Fe(1)–O(4)	89.88(10)
O(5A)–Fe(1)–O(11A)	91.21(11)	O(9)–Fe(1)–O(11A)	177.07(11)
O(8A)–Fe(1)–O(11A)	90.18(10)	O(1)–Fe(1)–O(11A)	87.01(11)
O(4)–Fe(1)–O(11A)	88.65(10)	P(1)–O(1)–Fe(1)	139.04(17)
P(2)–O(4)–Fe(1)	137.84(16)	P(2)–O(5)–Fe(1B)	149.80(17)
P(3)–O(8)–Fe(1B)	138.89(16)	P(3)–O(9)–Fe(1)	148.28(16)
P(4)–O(11)–Fe(1B)	137.30(16)		

Note. Symmetry transformations used to generate equivalent atoms: A: $-x+\frac{3}{2},y+\frac{1}{2},z$; B: $-x+\frac{3}{2},y-\frac{1}{2},z$.

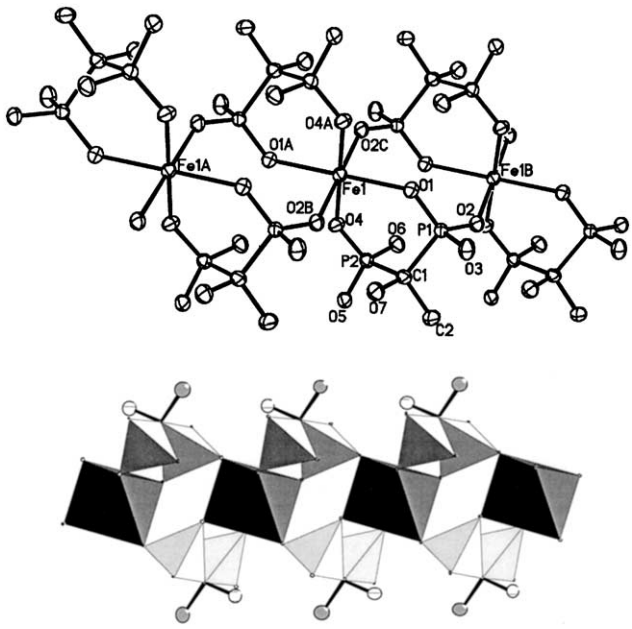

FIG. 1. A fragment of the chain in **1** with atomic labeling scheme (50% probability) (top) and with polyhedral representation (bottom). All H atoms are omitted for clarity.

TABLE 6
Hydrogen Bonds [Å, °] for 1 and 2

D–H···A	*d*(D–H)	*d*(H···A)	*d*(D···A)	<(DHA)
Compound **1**				
O(3)–H(3)···O(1W)	0.890(11)	1.758(12)	2.648(5)	179(4)
O(6)–H(6)···O(1)^{i}	0.888(10)	1.777(12)	2.665(4)	177(4)
O(7)–H(7)···O(2)^{ii}	0.98(5)	1.79(5)	2.755(4)	171(4)
O(1W)–H(1WA)···O(4)^{iv}	0.897(10)	1.899(16)	2.779(4)	166(4)
N(1)–H(1A)···O(5)^{v}	0.95(5)	1.94(5)	2.829(5)	156(4)
N(1)–H(1B)···O(7)^{iii}	0.91(5)	2.08(5)	2.939(5)	156(4)
N(1)–H(1C)···O(5)^{vi}	0.93(5)	1.82(5)	2.746(5)	169(4)
Compound **2**				
O(3)–H(1)···O(8)	0.893(10)	2.016(16)	2.886(4)	165(4)
O(7)–H(2)···O(11)^{i}	0.894(10)	1.847(12)	2.739(4)	175(4)
O(12)–H(6)···O(4)	0.893(10)	1.913(18)	2.772(4)	161(4)
O(14)–H(7)···O(1)^{ii}	0.896(10)	1.846(11)	2.741(4)	178(4)
O(1W)–H(1WA)···O(13)	0.895(10)	2.038(18)	2.916(5)	166(6)
O(1W)–H(1WB)···O(13)^{iii}	0.893(10)	2.21(4)	2.846(4)	128(4)
N(1)–H(23)···O(2)^{iv}	0.85(4)	2.04(4)	2.883(5)	171(7)
N(1)–H(22)···O(13)^{v}	0.87(5)	2.06(5)	2.910(5)	167(4)
N(1)–H(21)···O(2)	0.98(5)	1.91(5)	2.872(5)	167(4)
N(2)–H(29)···O(10)^{i}	0.89(4)	1.91(4)	2.716(4)	149(4)
N(2)–H(28)···O(6)^{vi}	0.93(4)	1.84(4)	2.667(4)	146(4)
N(3)–H(36)···O(6)^{vii}	0.80(5)	2.02(5)	2.758(5)	153(5)
N(3)–H(35)···O(10)	0.87(5)	1.95(5)	2.731(5)	149(4)
N(3)–H(34)···O(1W)^{vi}	0.79(5)	2.04(5)	2.825(5)	172(4)

Note. Symmetry transformations used to generate equivalent atoms:
For **1**: i: $-x,-y+1,-z$; ii: $x,y-1,z$; iii: $x,y+1,z$; iv: $x,-y,z+\frac{1}{2}$; v: $x,-y+1,z+\frac{1}{2}$; vi: $-x+\frac{1}{2},y+1/2,-z+\frac{1}{2}$.
For **2**: i: $-x+\frac{3}{2},y+1/2,z$; ii: $-x+\frac{3}{2},y-\frac{1}{2},z$; iii: $-x+2,y,-z+\frac{1}{2}$; iv: $-x+1,-y+1,-z$; v: $x-\frac{1}{2},-y+\frac{1}{2},-z$; vi: $x,-y+1,z-\frac{1}{2}$; vii: $-x+\frac{3}{2},-y+\frac{1}{2},z-\frac{1}{2}$.

Compound **2** crystallizes in space group *Pbcn*. It also exhibits a one-dimensional structure, composed of a $[Fe\{O_3PC(CH_3)(OH)(PO_3H)\}_2]_n^{3n-}$ anionic chain, a $[NH_3(CH_2)_2NH_2(CH_2)_2NH_3]^{3+}$ counterion, and a lattice water. An interesting feature of **2**, compared with **1**, is that the oxidation state of iron is +3, as indicated by the bond valence sum calculation of +3.02 and the Mössbauer spectrum as well. Considering that the same Fe source was used in the syntheses of **1** and **2**, the reason the oxidation state of Fe is different in the two compounds is not very clear. It could be related to the different templates used in the two cases. Consequently, the Fe–O bond lengths [1.950(3)–2.057(3)Å] in **2** are slightly shorter than those in **1**, but agree well with those in a ferric phosphonate, $HFe^{III}(C_6H_5PO_3H)_4$ [1.92–2.08Å] (7).

There are two independent $hedpH^{3-}$ groups in structure **2**. Each behaves as a tridentate chelating bridging ligand and coordinates to iron atoms in a way similar to hedp H_2^{2-} in **1**. The arrangements of the diphosphonate groups around iron, however, differ in the two structures. In compound **1**, two pairs of phosphonate oxygens [O(1) and O(4)] chelate the Fe atoms in a *trans*-mode (Fig. 1), whereas in **2**, similar pairs of phosphonate oxygens [O(1) and O(4), O(8A) and O(11A)] chelate in a *cis*-mode (Fig. 3). Unlike **1**, the phosphonate oxygens of each $hedpH^{3-}$ group in **2** is only singly protonated at O(3) or O(12) atom. Two phosphonate oxygens of each [O(2) and O(6), O(10) and O(13)] are pendant. Both are involved in the interchain hydrogen bond network with the protonated diethylenetriamine and the lattice water (Fig. 4 and Table 6). As a result, an entirely new type of chain structure is found in **2**, directed by diethylenetriamine.

Mössbauer Spectra and Magnetic Properties

The room temperature Mössbauer spectra for **1** and **2** are shown in Fig. 5. They can be least-squares fitted with one doublet corresponding to the one type of iron components observed in the two structures. The parameters δ (isomer shift) and ΔE_Q (quadrupole splitting) obtained are 1.68, 3.23 mm/s for **1** and 0.72, 0.42 mm/s for **2**, respectively. The former is typical of a high-spin Fe(II) ion (21, 22), and the latter is typical of a high-spin Fe(III) (11). These results agree well with the magnetic measurements.

Figure 6 shows the temperature-dependent magnetic susceptibilities for **1** in the forms of χ_m and χ_m^{-1} vs T plots. The effective magnetic moment at 298 K, calculated from $\mu_{eff} = 2.828(\chi_m T)^{1/2}$, is 5.88 μ_B per Fe, much higher than the spin-only value of 4.90 μ_B for $S = 2$. This high value is

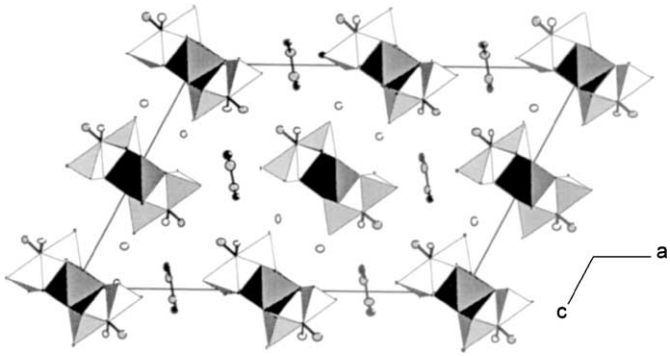

FIG. 2. Polyhedral representation of the structure **1** packed along the *b*-axis. All H atoms are omitted for clarity.

attributed to the orbital contribution of high-spin Fe(II) ions. The Weiss constant, determined in the temperature range 80 to 300 K, is −7.75 K, suggesting a weak antiferromagnetic exchange between the magnetic centers.

As described above, compound **1** exhibits a chain structure with the Fe(II) ions connected by the O–P–O bridges. The shortest Fe···Fe distance within the chain is

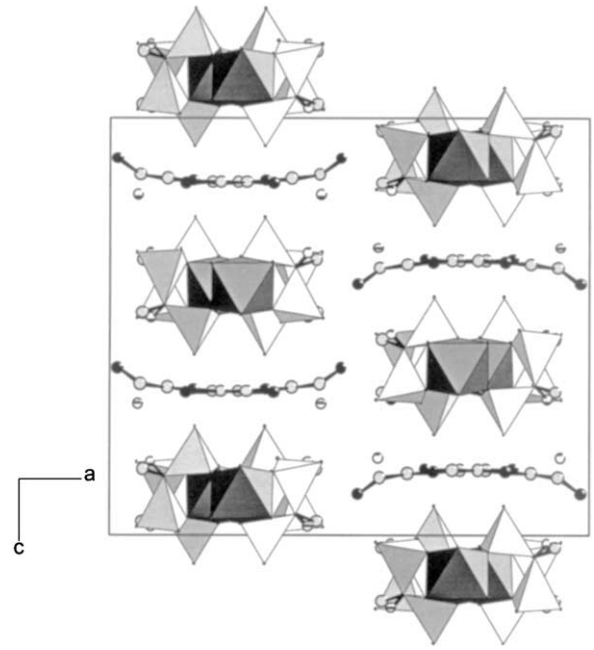

FIG. 4. Polyhedral representation of the structure **2** packed along *b*-axis. All H atoms are omitted for clarity.

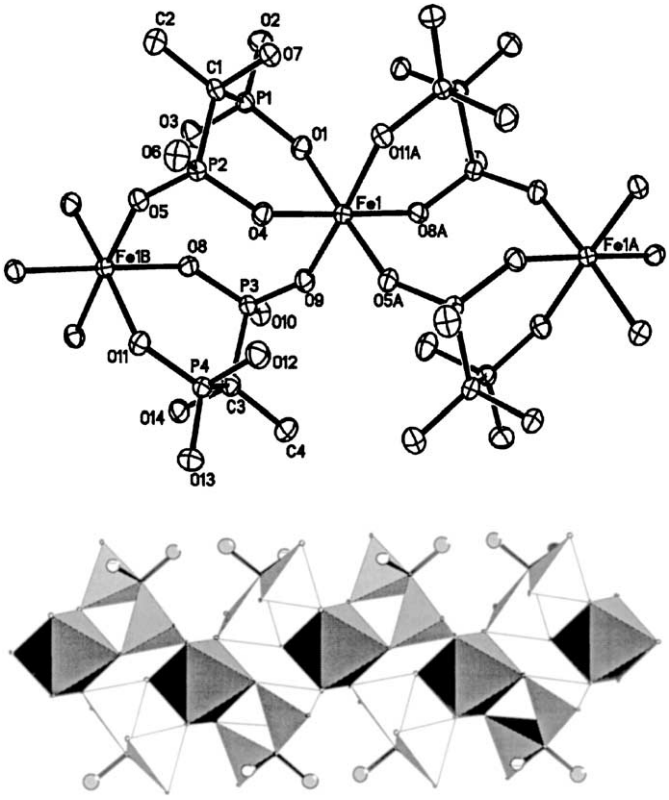

FIG. 3. A fragment of the chain in **2** with atomic labeling scheme (50% probability) (top) and with polyhedral representation (bottom). All H atoms are omitted for clarity.

5.331 Å over the O–P–O unit, excluding the possible direct exchanges between the iron ions. The superexchange coupling mediated through the O–P–O bridge is expected to be very weak. The susceptibility data could be analyzed by Fisher's expression for a uniform chain, with the classical spins scaled to a real quantum spin $S = 2$ (14, 23). A good fit was obtained, shown as the solid line in Fig. 6, with parameters $g = 2.41$, $J = -0.46$ cm^{-1}.

The magnetic behavior of compound **2** is shown in Fig. 7. The room temperature μ_{eff} (6.21 μ_B) per Fe is

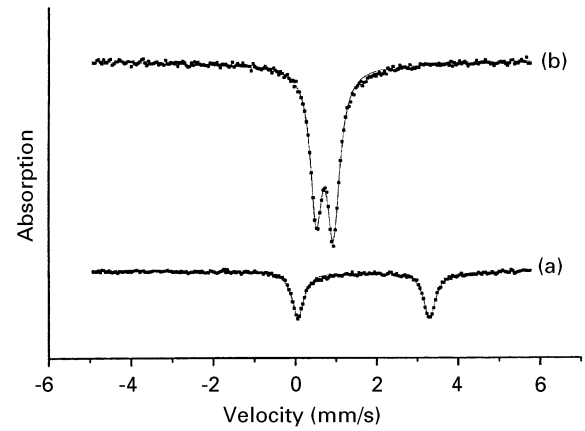

FIG. 5. Mössbauer spectra for **1** (a) and **2** (b)

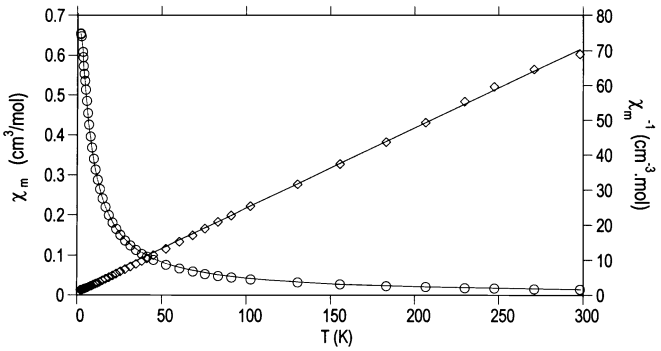

FIG. 6. The χ_m and $1/\chi_m$ vs T plots for **1**.

in agreement with the theoretical value ($5.91\,\mu_B$) for an $S=5/2$ ion. An antiferromagnetic exchange is again observed, featured by the maximum appearing in the χ_m vs T plot and the negative Weiss constant ($\theta=-16.3$ K) determined in the temperature range 60 to 300 K. Considering that compound **2** also has a chain structure where the Fe(III) instead of Fe(II) ions are bridged by the O–P–O groups, the magnetic data were analyzed by Fisher's expression with $S=5/2$. An excellent fit was obtained, shown as the solid line in Fig. 7, leading to parameters $g=2.09$, $J=-1.09$ cm^{-1}.

Thermal Analysis

The thermal analyses of compounds **1** and **2** have been performed in the temperature range 30–600°C. The compound **1** is thermally stable until about 140°C. Then it decomposes in approximately two steps. The weight loss below 340°C is 17.6%, corresponding to the release of two water molecules and one ethylenediamine molecule (calc. 17.1%). The second step of decomposition follows immediately with the collapse of the structure. For compound **2**, the decomposition starts at 120°C. The weight loss between 120 and 280°C is 1.5%, less than the calculated value (3.1%) for the removal of one water molecule. This could be due to the fact that the lattice water is involved in the extensive hydrogen bond networks in structure **2**. Above 280°C, compound **2** loses weight continuously in approximately two steps, similarly to **1**, suggesting that the structure collapses on removal of all the lattice water as well as the diethylenetriamine counterions.

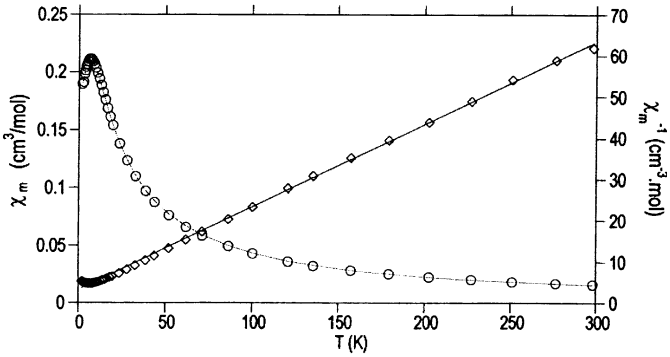

FIG. 7. The χ_m and $1/\chi_m$ vs T plots for **2**.

In conclusion, two new iron diphosphonate compounds, $[NH_3(CH_2)_2NH_3][Fe^{II}\{HO_3PC(CH_3)(OH)(PO_3H)\}_2]\cdot 2H_2O$ (**1**) and $[NH_3(CH_2)_2NH_2(CH_2)_2NH_3][Fe^{III}\{O_3PC(CH_3)(OH)(PO_3H)\}_2]\cdot H_2O$ (**2**), have been prepared under hydrothermal reaction conditions. The different organic templates used in the reactions direct the formation of two types of chain structures. Very weak antiferromagnetic interactions are found in both compounds.

ACKNOWLEDGMENTS

Support from the National Natural Science Foundation of China and the Analysis Center of Nanjing University is gratefully acknowledged. The authors also thank Dr. J.D. Korp, University of Houston, for crystallographic discussions.

REFERENCES

1. G. Cao, H. Hong, and T. E. Mallouk, *Acc. Chem. Res.* **25,** 420 (1992).
2. G. Alberti, "Comprehensive Supramolecular Chemistry" (J. M. Lehn, Ed.), Vol. 7. Pergamon, Elsevier, Oxford, 1996.
3. A. Clearfield, "Progress in Inorganic Chemistry" (K. D. Karlin, Ed.), Vol. 47, pp.371–510. Wiley, New York, 1998.
4. G. Huan, J. W. Johnson, A. J. Jacobson, and J. S. Merola, *J. Solid State Chem.* **89,** 220 (1990).
5. J. L. Snover, H. Byrd, E. P. Suponeva, E. Vicenzi, and M. E. Thompson, *Chem. Mater.* **8,** 1490 (1996).
6. G. Alberti, U. Constantino, M. Casciola, and R. Vivani, *Adv. Mater.* **8,** 291 (1996).
7. B. Bujoli, P. Palvadeau, and J. Rouxel, *Chem. Mater.* **2,** 582 (1990).
8. P. Palvadeau, M. Queignec, J. P. Venien, B. Bujoli and J. Villieras, *Mater Res. Bull.* **23,** 1561 (1988).
9. B. Bujoli, P. Palvadeau, and M. Queignec, *Eur. J. Solid State Inorg. Chem.* **29,** 141 (1992).
10. B. Bujoli, O. Pena, P. Palvadeau, J. Le Bideau, C. Payen, and J. Rouxel, *Chem. Mater.* **5,** 583 (1993).
11. M. Riou-Cavellec, C. Serre, J. Robino, M. Noguès, J.-M. Grenèche, and G. Férey, *J. Solid State Chem.* **147,** 122 (1999).
12. C. Bellito, F. Federici, S. A. Ibrahim, and M. R. Mahmoud, *Mater. Res. Soc. Symp. Proc.* **547,** 487 (1999).
13. L.-M. Zheng, H.-H. Song, C.-H. Lin, S.-L. Wang, Z. Hu, Z. Yu, and X.-Q. Xin, *Inorg. Chem.* **38,** 4618 (1999).
14. O. Kahn, "Molecular Magnetism" VCH, New York, 1993.
15. SAINT, "Program for Data Extraction and Reduction" Siemens Analytical X-Ray Instruments, Madison, WI, 1994–1996.
16. "SHELXTL (Version 5.0) Reference Manual." Siemens Industrial Automation, Analytical Instrumentation, Madison, WI, 1995.

17. D. Riou, P. Baltazar, and G. Férey, *Solid State Sci.* **2,** 127 (2000).
18. K. Barthelet, C. Jouve, D. Riou, and G. Férey, *Solid State Sci.* **2,** 871 (2000).
19. N. E. Brese and M. O'Keeffe, *Acta Crystallogr. Sec B.* **47,** 192 (1991).
20. H.-H. Song, L.-M. Zheng, C.-H. Lin, S.-L. Wang, X.-Q. Xin, and S. Gao, *Chem. Mater.* **11,** 2382 (1999).
21. F. Menil, *J. Phys. Chem. Solids,* **46,** 763 (1985).
22. J. T. Wrobleski and D. B. Brown, *Inorg. Chem.* **18,** 2738 (1979).
23. M. E. Fisher, *Am. J. Phys.* **32,** 343 (1964).